SUPPLEMENTAL MATERIAL

STROBE Statement-Checklist

	No.	Recommendation	
Title and abstract	1	(a) indicate the study's design with a commonly used term in the title or the abstract	P1L10
		(b) Provide in the abstract an informative and balanced summary of what was done and what was found	P1-2
Introduction			
Background/rationale	2	Explain the scientific background and rationale for the investigation being reported.	P3L2-P4L2
Objective	3	State specific objectives, including any prespecified hypotheses	P4L5-9
Methods			
Study design	4	Present key elements of study design early in the paper	P4L11-19
Setting	5	Describe the setting, locations, and relevant dates, including periods of recruitment, exposure, follow-up, and data collection	P4L11-19
Participants	6	*(a)* Give the eligibility criteria, and the sources and methods of selection of participants	supplemental material P4L3-11
Variables	7	Clearly define all outcomes, exposures, predictors, potential confounders, and effect modifiers. Give diagnostic criteria, if applicable	P4L11-14
Data sources/ measurement	8	For each variable of interest, give sources of data and details of methods of assessment (measurement). Describe comparability of assessment methods if there is more than one group	supplemental material P5L5-P8L13
Bias	9	Describe any efforts to address potential sources of bias	N/A
Study size	10	Explain how the study size arrived at	supplemental material P4L3-11
Quantitative variables	11	Explain how quantitative variables were handled in the analyses. If applicable, describe which grouping were chosen and why	N/A
Statistical methods	12	(*a*) Describe all statistical methods, including those used to control for confounding	supplemental material P8L15-P9L10
		(*b*) Describe any methods used to examine subgroups	N/A

		and interactions	
		(*c*) Explain how missing data were addressed	supplemental material P4L10-11
		(*d*) If applicable, describe analytical methods taking account of sampling strategy	N/A
		(*e*) Describe any sensitivity analyses	N/A
Results			
Participants	13	(*a*) Report numbers of individuals at each stage of study – e.g. numbers potentially eligible, examined for eligibility, confirmed eligible, included in the study, completing follow-up, and analysed	P5L3
		(*b*) Give reasons for non-participation at each stage	N/A
		(*c*) Consider use of a flow diagram	P4L16
Descriptive data	14	(*a*) Give characteristics of study participants (e.g. demographic, clinical, social) and information on exposures and potential confounders	P5L3-4
		(*b*) Indicate number of participants with missing data for each variable of interest	supplemental material P4L10-11
Outcome data	15*	Report numbers of outcome events or summary measures	N/A
Main results	16	(*a*) Give unadjusted estimates and, if applicable, confounder-adjusted estimates and their precision (e.g. 95% confidence interval). Make clear which confounders were adjusted for and why they were included	N/A
		(*b*) Report category boundaries when continuous variables were categorized	N/A
		(*c*) If relevant, consider translating estimats of relative risk into absolute risk for a meaningful time period	N/A
Other analyses	17	Report other analyses done – e.g. analyses of subgroups and interactions, and sensitivity analyses	N/A
Discussion			
Key results	18	Summarise key results with reference to study objectives	P9L21-P10L8
Limitation	19	Discuss limitations of the study, taking into account sources of potential bias or imprecision. Discuss both direction and magnitude of any potential bias	P13L18-P14L3
Interpretation	20	Give a cautious overall interpretation of results considering objectives, limitations, multiplicity of analyses, results from similar studies, and other relevant evidence	P11L11-P13L17

Generalisability	21	Discuss the generalisability (external validity) of the study resultes	P14L1-3
Other information			
Funding	22	Give the source of founding and the role of the founders for the present study and, if applicable, for the original study on which the present article is based	P14L13-14

Supplemental Methods

Participants

Enrolled into this study were the consecutive patients who had CT-confirmed unilateral spontaneous basal ganglia ICH (> 18 years) and had received magnetic resonance angiography (MRA)/computed tomography angiography (CTA) (within 7 days of onset) in Union Hospital, Tongji Medical College, Huazhong University of Science and Technology, Wuhan, China, between September 1, 2013 and June 30, 2019. The clinical data of the patients were collected from the institutional medical database. Those who had secondary ICH, softening range in the basal ganglia, dementia, no M1 segment, and poor imaging data were excluded. Patients whose data were missing or not available were also eliminated. The flow diagram for patient selection is shown in Figure 1. All patients' MRA/CTA images were analyzed from the ipsilateral side, with the contralateral side serving as a self-control, to study the high-risk features of ICH. The requirement for informed consent from patients was waived by the ethics committee due to the retrospective nature of the study. The data are anonymous, and all authors could only use the anonymized data for statistical analysis. STROBE was used as the reporting guideline and no extensions were used.

Neuroimaging Data

MRI was performed on a 3.0-tesla system (SIEMEHS) equipped with adequate head coils. The protocol included conventional 3-dimensional time-off light MRA, T1-weighted imaging, and T2-weighted imaging of the head. Maximum intensity projection (MIP) images were reconstructed from 3-dimensional time-off light MRA

on axial, sagittal and coronal planes in all patients. CT was performed on a 64-slice system (PHILIPS-CX). The protocol involved conventional CTA and plain CT scan of the head. MIP images were reconstructed from CTA on axial, sagittal and coronal planes in all patients.

The parameters used in our study included the MCA-related variables and other items that might be related to spontaneous basal ganglia ICH. All the parameters were measured on the Picture Archiving and Communication System. The MCA-related geometric features examined included M1 length, M1 proximal/distal diameter, shape of M1, M1 curve orientation, M1/M2 angle and MCA bifurcation angle (Figure 2A-D). M1 length and proximal/distal diameter were measured on axial plane. Shape of M1 was categorized as straight or curved based on axial and coronal MIP images of 3-dimensional time-off light MRA/CTA. We determined the orientation of the curved M1 on the basis of the direction(s) in which each M1 curve opened and measured the angle in the two directions respectively. Ventral- and dorsal-oriented M1 curves were identified by using axial MIP images, while superior- and inferior-oriented M1 curves were identified using coronal MIP images. The M1/M2 angle (the angle between M1 segment and the plane where the M2 branches were on) and MCA bifurcation angle (the angle of two M2 branches; all have two branches in our cases) were measured in different directions to fully present the relative position among the vessels. Windowing for the 3D reconstructions was validated against the multiplanar reconstructions to ensure accurate measurement.

Other parameters included the hematoma volume, and presence (or absence) of

intraventricular extension, aneurysm(s) in the adjacent vessels and stenosis of the M1 segment. The hematoma volume was measured in Picture Archiving and Communication System. The researcher manually outlined the hematoma and then the system calculated the volume automatically.

Images were analyzed twice by a researcher who was blind to all clinical information, with the two analyses being 1 month apart. To evaluate the consistency between examiners, another image reader, also blind to all clinical data, assessed 50 imaging materials randomly and independently selected from the overall imaging materials.

Control Equation of the Blood Flow in the Cerebral Vessels

Hemodynamically, the Naviers-Stokes equation, continuity equation, and motion equation of incompressible viscous fluids are commonly used to describe blood flow. The basic mechanical laws of viscous fluid flow are described, and the formulae were as follows:

(1) Naviers-Stokes equation

$$\frac{\partial v}{\partial t} + (v \bullet \Delta)v = -\frac{1}{\rho}\Delta p + \frac{\eta}{p}\Delta^2 v$$

where, v represents fluid velocity, ρ fluid density, p pressure, and η hemodynamic viscosity.

(2) Continuity equation

$$\frac{\partial u}{\partial x} + \frac{\partial v}{\partial y} + \frac{\partial w}{\partial z} = 0$$

where *u*, *v*, and *w* are the velocity components of the velocity vector on *x*, *y*, and *z*, respectively.

(3) Momentum conservation equation

$$\frac{\partial(\rho u)}{\partial t}+div(\rho uU)=div(\eta gradu)+Su-\frac{\partial p}{\partial x}$$
$$\frac{\partial(\rho v)}{\partial t}+div(\rho vU)=div(\eta gradv)+Sv-\frac{\partial p}{\partial y}$$
$$\frac{\partial(\rho w)}{\partial t}+div(\rho wU)=div(\eta gradw)+Sw-\frac{\partial p}{\partial z}$$

where, *u*, *v,* and *w* are the velocity components of the velocity vector on *x*, *y,* and *z*, respectively, and η is the dynamic viscosity of the fluid; *Su*, *Sv,* and *Sw* are the broad source terms of the three momentum conservation equations, respectively.

(4) Fluid properties

In the study, blood was seen as an incompressible Newtonian fluid, with blood density ρ=1050 kg/m^3 and viscosity=0.0024 Pa·s (in ref 10, the viscosity was set at 0.0035, being virtually identical to the parameter used in the present paper). This study ignored the influence of gravity in the simulation, and the vascular wall was taken as a non-viscoelastic rigid wall under the condition of no slip referring to the previous studies. [1-3] The inner diameter at the entrance of M1 segment was within 2.1~2.7 mm. We enrolled 158 patients, the peak blood velocity in the brain was 0.4~1.1 m/s, and the peak Re of Re=$\rho vD/\mu$ number was 367~1300. Therefore, in the numerical simulation, the blood movement in the cerebral artery was assumed to be a steady laminar flow, and the inlet flow rate was defined as 5e-6 m^3/*s*.

(5) Geometric model, mesh and boundary conditions

In the analysis with the scFLOW module from MSC Cradle, the grid was first divided based on the scFLOW Preprocessor software. Due to the irregularity and complexity of the model, the unstructured octree method was adopted to divide it, and the grid was of polyhedral type. The meshes were divided into intelligent meshes, i.e., when the geometric shapes change, the meshes divided automatically and reasonably according to the geometric shapes encountered, so as to obtain a relatively optimal mesh cell. For MCA meshing, non-equidistant meshing along the radius direction was adopted to improve the calculation accuracy of the boundary layer of the pipe wall, while for all LSAs, non-equidistant meshing was used and local refinement was performed at each bifurcation point to improve the accuracy. There were roughly 1.35 million units in the model (supplementary Figure 1), and the convergence is also provided and discussed in this paper. Furthermore, the mesh data including the boundary layer zone, are also detailed in supplementary Figure 5.

Statistical analysis

Statistical analysis was performed by employing Statistical Product and Service Solutions 12.0 for Windows. For descriptive analysis, frequency and percentage were used for independent variables. The paired *t*-test was employed to compare quantitative data of the MCA geometric features. The Bowker test was utilized to compare enumeration data of the MCA geometric features. Then, multivariate logistic regression analysis was conducted to identify the association between the MCA geometric features and hematoma volume. Variables input into the model included age, gender, smoking and drinking habits, hypertension, diabetes mellitus,

hypercholesterolemia, coronary artery disease, previous ischemic stroke, previous ICH, time of scanning, intraventricular extension and the geometric features of MCA. The relationship between the MCA geometric features and NIHSS score was also examined by multivariate logistic regression. Variables input into the model were age, gender, smoking and drinking habits, hypertension, diabetes mellitus, hypercholesterolemia, coronary artery disease, previous ischemic stroke, previous ICH, time of scanning, intraventricular extension, hematoma volume and the MCA geometric features. Adjusted odds ratios (ORs) and 95% confidence intervals (CIs) for variables were obtained. For all analyses, differences were tested using two-tailed tests, and a $P<0.05$ was considered to be statistically significant.

Supplemental references

1. Leng X, Lan L, Ip HL, et al. Hemodynamics and stroke risk in intracranial atherosclerotic disease. Ann Neurol. 2019 May;85(5):752-764.
2. Leng X, Scalzo F, Ip HL, et al. Computational fluid dynamics modeling of symptomatic intracranial atherosclerosis may predict risk of stroke recurrence. PLoS One. 2014 May 12;9(5):e97531.
3. Liu J, Yan Z, Pu Y, et al. Functional assessment of cerebral artery stenosis: a pilot study based on computational fluid dynamics. J Cereb Blood Flow Metab. 2017 Jul;37(7):2567-2576.

Supplemental Tables

Table 1 shows determinants associated with hematoma volume. Patients who had suffered hypertension had larger hematoma volume (β=9.83, SE=4.93, *P*=0.0492), while patients who had intraventricular extension had smaller hematoma volume (β=-13.22, SE=3.80, P=0.0008). Other covariates, including MCA geometric features, showed no significant differences in multivariable linear regression analysis.

Covariate	**Intracerebral Hemorrhage Volume**	
	β (SE)	***P* Value**
Age	-0.18 (0.17)	0.3143
Gender	-1.11 (4.45)	0.8045
Smoking	-0.27 (4.60)	0.9539
Drinking	-1.58 (4.40)	0.7208
Hypertension	9.83 (4.93)	0.0492
Diabetes mellitus	6.81 (7.44)	0.3625
Hypercholesterolemia	0.97 (5.21)	0.8523
Coronary artery disease	-6.96 (9.21)	0.4519
Previous ischemic stroke	7.77 (7.52)	0.3044
Previous ICH	15.88 (10.78)	0.1444
Time to scan	0.14 (0.11)	0.2153
Intraventricular extension	-13.22 (3.80)	0.0008
M1 length	0.42 (0.30)	0.1572
M1 diameter ratio (proximal/ distal)	-14.54 (8.85)	0.1041

M1 shape and curve orientation (axial)	-3.45 (6.46)	0.5952
Bending angle (axial)	0.01 (0.18)	0.9347
M1 shape and curve orientation (coronal)	-2.16 (6.61)	0.7446
Bending angle (coronal)	0.16 (0.09)	0.0886
M1/M2 angle	0.02 (0.08)	0.8276
MCA bifurcation angle	-0.06 (0.07)	0.4325

Table 2 shows determinants associated with NIHSS score. Predictors of NIHSS score identified through multivariable linear regression analysis were age and hematoma volume. The older patients (β=0.27, SE=0.11, *P*=0.0161) and those who had larger hematoma volume (β=0.26, SE=0.06, *P*=0.0002) had higher NIHSS score. Other covariates, including MCA geometric features, were not associated with NIHSS score.

Covariate	**NIHSS score**	
	β (SE)	***P* Value**
Age	0.27 (0.11)	0.0161
Gender	2.29 (2.87)	0.4269
Smoking	1.97 (2.72)	0.4721
Drinking	-0.60 (2.72)	0.8278
Hypertension	0.80 (3.20)	0.8023
Diabetes mellitus	4.67 (4.69)	0.3241
Hypercholesterolemia	2.85 (3.07)	0.3570
Coronary artery disease	-3.72 (5.90)	0.5312
Previous ischemic stroke	4.01 (5.13)	0.4380
Previous ICH	2.72 (11.47)	0.8133
Time to scan	0.09 (0.21)	0.6527
Intraventricular extension	-4.72 (2.39)	0.0528
Hematoma volume	0.26 (0.06)	0.0002
M1 segment length	-0.16 (0.21)	0.4485

M1 segment diameter ratio (proximal/ distal)	3.76 (5.39)	0.4886
M1 segment shape and curve orientation (axial)	2.88 (4.04)	0.4785
Bending angle (axial)	-0.07 (0.12)	0.5756
M1 segment shape and curve orientation (coronal)	1.62 (3.74)	0.6659
Bending angle (coronal)	0.08 (0.06)	0.2090
M1/M2 angle	-0.03 (0.05)	0.5760
MCA bifurcation angle	-0.06 (0.05)	0.1716

Table3. The diverge of the convergence with different element sizes

	Core	Medium	Fine
Pin	691665	73052	738300
Mesh size[m]	0.0005	0.00025	0.00018
Element number	280000	1340000	2180000

Supplemental Figures and Figure Legends

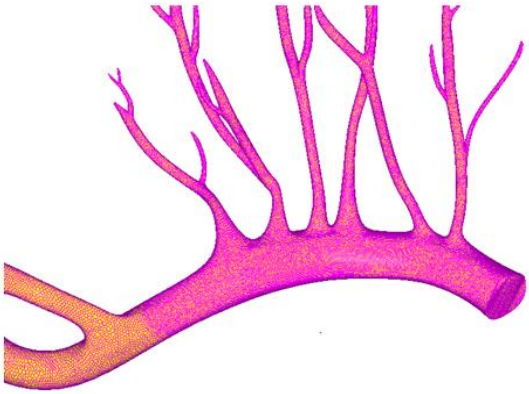

Figure 1 Numerical computational mesh model

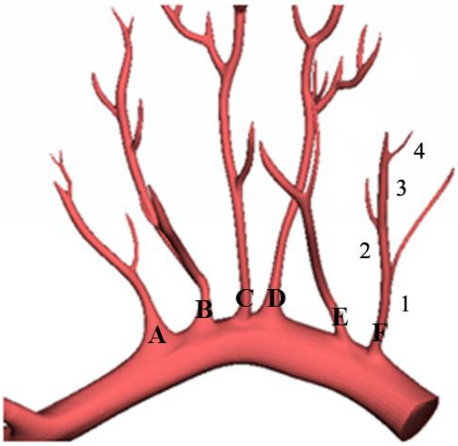

Figure 2 Geometrical characteristics of the lenticular artery.

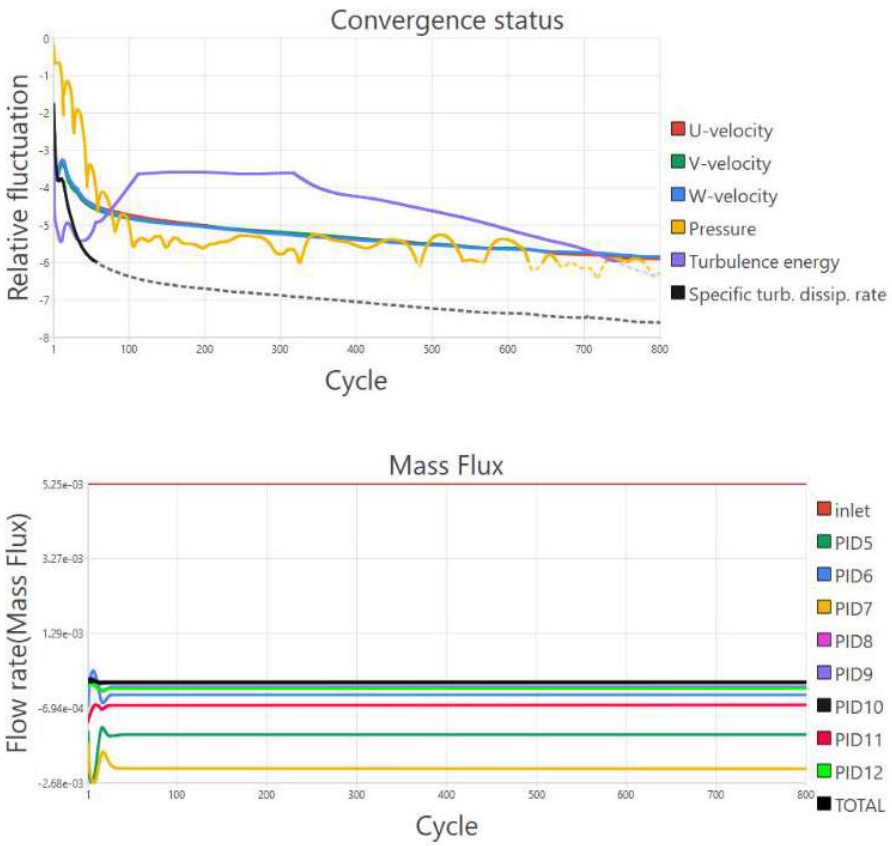

Figure 3. Convergence of the CFD simulation

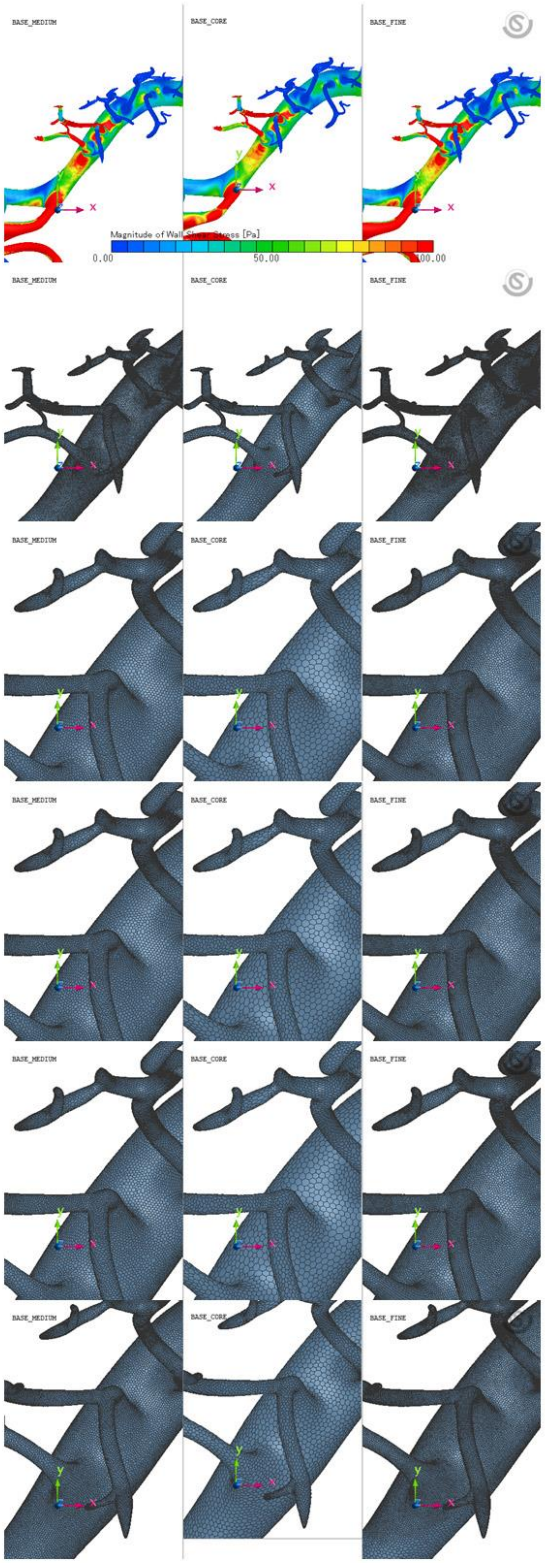

Figure 4. The simulation results with different element sizes

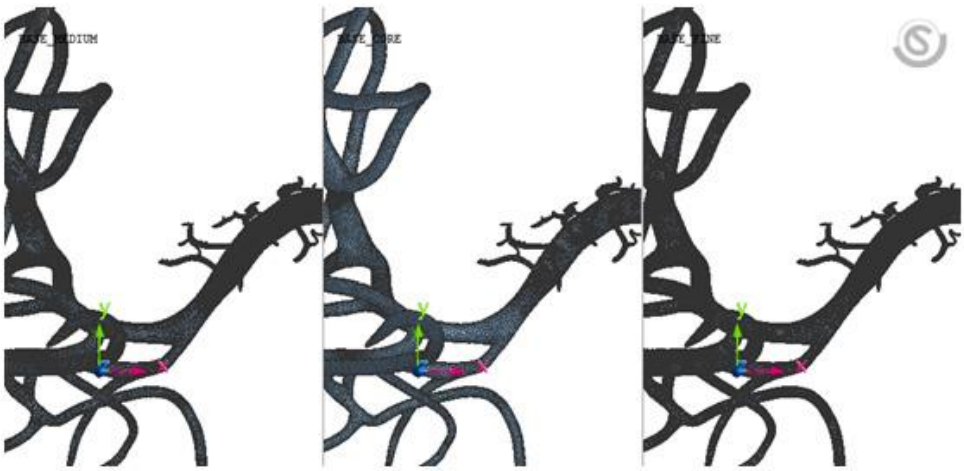

Figure 5. The mesh pattern in the boundary layer zone

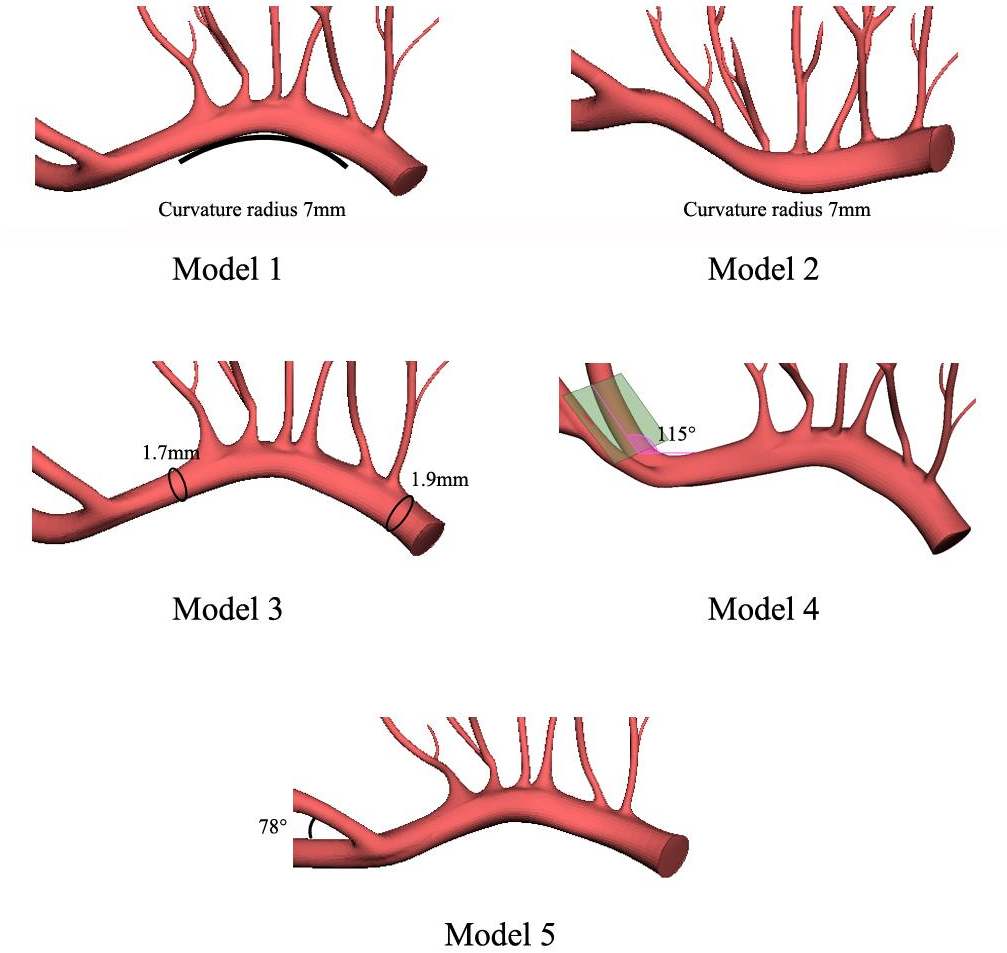

Figure 6 Reconstruction model of lesion features. Model 1: the superior-oriented M1. Model 2: the superior-oriented M1. Model 3: increased M1 segment diameter ratio (proximal/ distal). Model 4: decreased M1/M2 angle. Model 5: decreased MCA bifurcation angle.

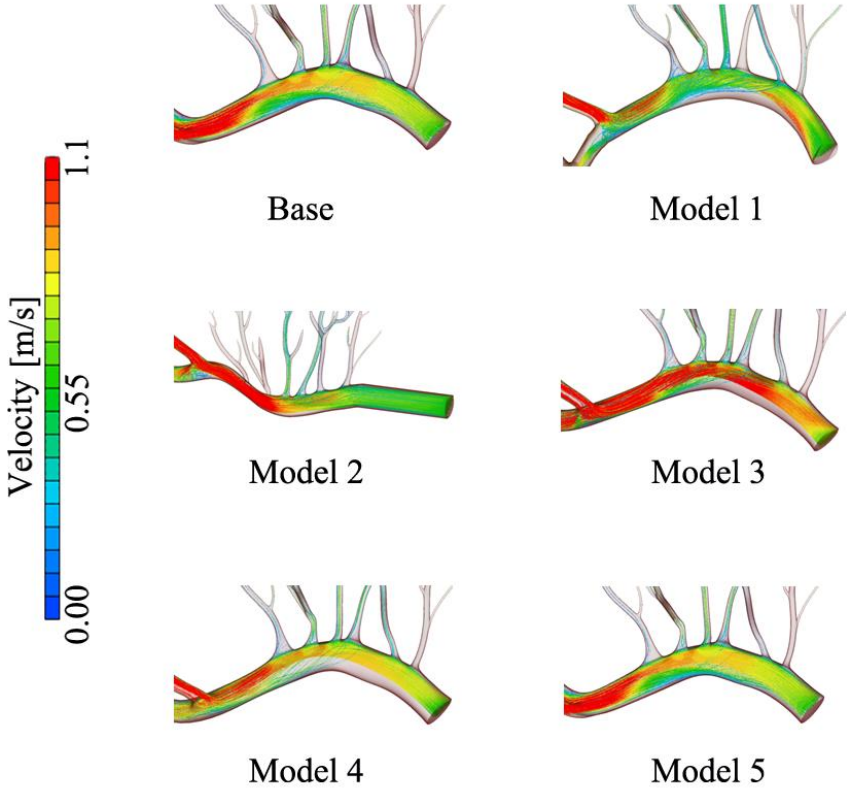

Figure 7 Blood flow chart. The blood flow in MCA and LSAs were essentially in a stable laminar flow state, and the blood flow was stable and relaxed. According to the simulation results of various models, the distal flow velocity of M1 segment was high. The M1 segment bent superior and a low-speed zone was formed in the middle of the M1 segment. In the inferior-oriented characteristic model of M1 segment, the bending curvature of M1 segment becomes smaller and the velocity increased. For the working condition of Model 3, the flow velocity in vessel increased. The decrease in the M1/M2 angle led to a decreased blood flow velocity at the distal end of M1 segment. It can be seen from the working condition of Model 5 where the change of the MCA bifurcation angle exerted no influence on the flow velocity.